Evidence for chimney breakout in the Galactic supershell GSH 242-03+37

N. M. McClure-Griffiths,[1] Alyson Ford,[1,2] D. J. Pisano,[3,4] B. K. Gibson,[2,5,6] L. Staveley-Smith,[1] M. R. Calabretta,[1] L. Dedes,[7] and P. M. W. Kalberla[7]

ABSTRACT

We present new high resolution neutral hydrogen (H I) images of the Galactic supershell GSH 242-03+37. These data were obtained with the Parkes Radiotelescope as part of the Galactic All-Sky Survey (GASS). GSH 242-03+37 is one of the largest and most energetic H I supershells in the Galaxy with a radius of 565 ± 65 pc and an expansion energy of 3×10^{53} ergs. Our images reveal a complicated shell with multiple chimney structures on both sides of the Galactic plane. These chimneys appear capped by narrow filaments about 1.6 kpc above and below the Galactic mid-plane, confirming structures predicted in simulations of expanding supershells. The structure of GSH 242-03+37 is extremely similar to the only other Galactic supershell known to have blown out of both sides of the plane, GSH 277+00+36. We compare the GASS H I data with X-ray and H-α images, finding no strong correlations.

Subject headings: surveys — Galaxy: structure — ISM: structure — ISM: Bubbles — ISM: H I

[1]Australia Telescope National Facility, CSIRO, PO Box 76, Epping NSW 1710, Australia; naomi.mccluregriffiths@csiro.au

[2]Centre for Astrophysics and Supercomputing, Swinburne University of Technology, Hawthorn VIC 3122, Australia

[3]Remote Sensing Division, Naval Research Laboratory, Code 7213, 4555 Overlook Ave. SW, Washington, D.C, 20375

[4]National Research Council Postdoctoral Fellow

[5]Laboratoire d'Astrophysique, Ecole Polytechnique Federale de Lausanne (EPFL), Observatoire, CH-1290, Sauverny, Switzerland

[6]Centre for Astrophysics, University of Central Lancashire, Preston, PR1 2HE, United Kingdom

[7]Radioastronomisches Institut der Universität Bonn, Auf dem Hügel 71, 53121 Bonn, Germany

1. Introduction

Among the most dramatic structures in the interstellar medium (ISM) of disk galaxies are large shells and supershells. These objects are generally observed as voids in the neutral hydrogen (H I) distribution surrounded by swept-up walls. In some nearby galaxies, like the Large and Small Magellanic Clouds, the H I structure of the disk is dominated by shells and supershells (Kim et al. 1999; Hatzidimitriou et al. 2005). The ISM of the Milky Way is also riddled with tens, if not hundreds, of H I shells (e.g. Heiles 1979, 1984; McClure-Griffiths et al. 2002; Ehlerová & Palouš 2005). It is thought that most H I shells are formed by stellar winds or supernovae, or the combined effects of both. This explanation is particularly convincing for smaller shells, with diameters of a few tens of parsecs and formation energies on the order of 10^{52} ergs. However, the larger shells, or supershells, are enigmatic. They seem to require unreasonably large ($> 10^{53}$ ergs) formation energies in order to maintain expansion velocities of ~ 20 km s^{-1} at radii in excess of a few hundred parsecs (Heiles 1984). The stellar wind and supernova from a given massive star is capable of injecting $\sim 10^{51}$ ergs of energy into the ISM, suggesting that many hundreds and even thousands of massive stars are required to power the most energetic shells. In this case, it is expected that multiple generations of star formation are required, and although numerous studies have searched for evidence of triggered star formation associated with H I shells there are few examples (Oey et al. 2005).

H I supershells play a significant role in the energy budget of the ISM and can also play a role in the exchange of matter between the disk and halo. H I supershells can grow large enough to exceed the scale height of the H I disk. In this case, the shell expands rapidly along the density gradient away from the disk until it becomes unstable and breaks out, venting its hot internal gas to the halo. This "chimney" process may provide a mechanism for distributing hot gas and metals away from the disk (Dove, Shull, & Ferrara 2000). H I shell blow-outs are predicted for, and indeed observed in, a number of dwarf galaxies where the gravitational potential of the disk is smaller than in large spirals (Mac Low & Ferrara 1999; Marlowe et al. 1995). Occasionally chimneys are observed in large spiral galaxies, with good examples being NGC 891, NGC 253 and NGC 6946 (Rand et al. 1990; Howk & Savage 1997; Boomsma et al. 2005). In the Milky Way, very little is known about the impact of chimneys on the formation, structure and dynamics of the halo. In fact, only a handful of relatively small chimneys are known in the Milky Way, e.g. the Stockert chimney (Müller et al. 1987), the W4 chimney (Normandeau et al. 1996; Reynolds et al. 2001), the Scutum supershell (Callaway et al. 2000) and GSH 277+00+36 (McClure-Griffiths et al. 2000). Together, the known chimneys are not capable of providing the thermal energy required to support the halo.

One of the largest H I supershells in the Milky Way is GSH 242-03+37, discovered by Heiles (1979) in his seminal work on Galactic shells. GSH 242-03+37 is located at $l = 242°$, $b = −3°$, which is in the direction of the so-called "Puppis window", an area of very low visual extinction (Fitzgerald 1968). The shell has an angular diameter of 15°. Its kinematic distance is 3.6 kpc, implying a physical diameter of ~ 1 kpc. Heiles (1979) suggested that GSH 242-03+37 is still expanding with an expansion velocity of $v_{\mathrm{exp}} \approx 20$ km s^{-1} and from that he estimated an expansion energy of $E_E \sim 1.6 \times 10^{54}$ ergs. Despite the impressive size and implied energetics of this shell, there has been very little follow-up work. Stacy & Jackson (1982) made a thorough study of the H I in the region $239° \leq l \leq 251°$ with the aim of correlating H I features with optical spiral tracers. The survey concentrated mainly on smaller scale H I features, and while it mentioned GSH 242-03+37, no detailed images were available or discussed.

Here we use new data from the Galactic All-Sky Survey (GASS) to study the H I supershell GSH 242-03+37. We present the highest angular resolution ($\sim 15'$) and most sensitive images of the shell published so far. We show that GSH 242-03+37 has in fact broken out of both sides of the Galactic plane through three large channels. We show that these chimney openings are capped at high Galactic latitude with very narrow, low surface brightness filaments. We discuss the chimney caps and their long-term fate in §4.3. In §3.3 we examine archival X-ray (ROSAT) and H-alpha (SHASSA) data to explore the various gas phases associated with the chimney. In §4.1 we discuss the stellar content of the shell and in §4.2 we explore the possible association of a small shell that appears inside GSH 242-03+37.

2.   Observations and Analysis

The H I data presented here are from the first pass of the Parkes Galactic All-Sky Survey (GASS; McClure-Griffiths et al., 2005, in prep.). GASS is a project to image H I at Galactic velocities (-400 km s$^{-1} \leq v_{\mathrm{LSR}} \leq +450$ km s^{-1}) for the entire sky south of declination $0°$. GASS uses the Parkes multibeam to produce a fully sampled atlas of H I with an angular resolution of $15'$, spectral resolution of 0.8 km s^{-1}, and to an rms sensitivity of 80-90 mK. The survey will be corrected for stray radiation effects, according to the method described in Kalberla et al. (2005), to ensure high reliability of the H I spectra. Observations for the survey began in January 2005 and will continue through to 2007. When complete, GASS will be the first fully sampled all-sky survey of H I on sub-degree scales. The full survey details, including its scientific goals, will be described in a future paper. Here we briefly describe the observations and data reduction techniques to allow assessment of the data presented.

GASS is conducted as an on-the-fly mapping survey, with each point in the sky scanned

twice. We use the Parkes multibeam (Staveley-Smith et al. 1996), which is a thirteen beam receiver package mounted at prime focus on the Parkes Radiotelescope near Parkes NSW, Australia. The thirteen beams of the multibeam are packed in a hexagonal configuration with a beam separation on the sky of 29′.1 for the inner beams. On-the-fly mapping is performed by scanning the telescope at a rate of 1 deg min^{-1}, recording spectra every 5 seconds. While scanning, the receiver package is rotated by 19°.1 with respect to the scan direction to ensure that the inner seven independent beams make parallel tracks equally spaced by 9′.5 on the sky. Scans in both right ascension and declination will be made for the full survey, although only a few RA scans have been included in this paper. The declination scans are made at a constant RA and are 8 deg long in declination. After a scan the receiver package is offset in RA to perform an interleaved scan, reducing the spacing between adjacent beam tracks to 4′.7.

Spectra are recorded in a special correlator mode that allows 2048 channels across an 8 MHz bandwidth on all thirteen beams. In-band frequency switching is used to allow for robust bandpass correction. We switch every 5 seconds between center frequencies of 1418.8345 MHz and 1421.9685 MHz. Bandpass calibration is done in near real-time using the *Livedata* package, which is part of the ATNF subset of the *aips++* distribution. The bandpass correction algorithm employed was designed expressly for the GASS frequency-switched data. It works on each beam, polarization and IF independently, performing a robust polynomial fit to the quotient spectrum (one frequency divided by the second frequency) after masking the emission by examining the spectrum both spectrally and spatially. *Livedata* also performs the Doppler correction to shift the spectra to the Local Standard of Rest (LSR). Absolute brightness temperature calibration was performed from daily observations of the IAU standard line calibration regions S8 and S9 (Williams 1973).

Calibrated spectra are gridded into datacubes using the *Gridzilla* package, also part of the ATNF subset of the *aips++* distribution. The gridding algorithm used in *Gridzilla* is described in detail in Barnes et al. (2001). GASS spectra were imaged using a weighted median technique with a cell size of 4′, a Gaussian smoothing kernel with a full width half max of 12′, and a cutoff radius of 8′. The effective resolution of the gridded data is ∼ 15′. The per channel rms of the resulting image cubes near the Galactic plane is ∼ 120 mK. These data are not corrected for stray radiation and may therefore contain some low-level spurious features. For the data presented here we have compared our images with the low resolution stray radiation corrected Leiden/Argentine/Bonn survey (Kalberla et al. 2005; Bajaja et al. 2005) to verify features.

3. Results

Heiles (1979) cataloged GSH 242-03+37 with a low confidence rating, suggesting uncertainty about the shell's veracity. With the improved angular and spectral resolution of the GASS data, as well as the availability of improved data visualization tools, we are confident that this shell meets the three criteria for shell identification given in McClure-Griffiths et al. (2002), i.e. that the void is well-defined over more than three consecutive velocity channels with an interior to exterior brightness contrast of 5 or more, that the void changes shape with velocity and that a velocity profile through the shell shows a well-defined dip flanked by peaks.

In Figure 1 we show velocity channel images of the shell as multiple panels. The shell is visible as the large void in the center of the images, between LSR[1] velocities $v \approx 30$ km s^{-1} and $v \approx 50$ km s^{-1}. Every fourth velocity channel is displayed here to give an impression of the dynamic structure in the shell. The first and last panels of Fig. 1 show the approximate front and back caps of the shell. The shell extends over approximately 18 degrees in longitude and 10 degrees in latitude. However, there are clear breaks on the top and bottom of the shell, as seen in the velocity channel images. These are indicative of chimney openings and will be discussed thoroughly below. We find that the center of the shell is at a slightly different location than given in Heiles (1979). We define the center as the velocity of least emission in the spectral profile through the shell center and the geometric center of the shell at that velocity. Using these criteria, the center of the shell is at $l = 243°$, $b = -1.6°$, $v = +42$ km s^{-1}, notably different than the coordinates implied by its name.

A velocity profile through the shell center is shown in the top panel of Figure 2. The shell is the clearly defined dip in the profile at $v \approx 40$ km s^{-1}. The front and back caps of the shell are marked on Fig. 2 and are apparent as the bumps in the velocity profile at $v \approx 27$ km s^{-1} and $v \approx 57$ km s^{-1} on both sides of the void. The shell is located at a Galactic longitude where the rotation curve is relatively simple, allowing us to translate radial velocity approximately into distance. The lower panel of Fig. 2 plots the velocity-distance relation at $l = 244°$ from the Brand & Blitz (1993) rotation curve, assuming the IAU recommended values for the Galactic center distance, $R_0 = 8.5$ kpc, and LSR velocity, $\Theta_0 = 220$ km s^{-1}. From this relationship the kinematic distance of the shell is 3.6 kpc, as was also found by (Heiles 1979). The shell is at a Galactocentric radius of $R_g = 10.7$ kpc. The error on the kinematic distance is on the order of 10% because of uncertainties in determining the central velocity of the shell, random cloud-to-cloud motions in the ISM and errors in the rotation curve. The radius of the shell along the plane is $R_{sh} = 565 \pm 65$

---

[1]All velocities are quoted with respect to the kinematic Local Standard of Rest.

pc. At a distance of 3.6 kpc our resolution is approximately 16 pc. Because of the large size of the shell it may be elongated because of differential rotation in the Galactic plane (Tenorio-Tagle & Bodenheimer 1988). This will distort the shell and affect its lifetime as discussed below.

The interior of the shell has extremely low brightness temperature values when compared with the rest of the Galactic plane; the mean brightness temperature in the shell interior is only $T_{\rm b} = 4$ K with a standard deviation on the mean of $\sigma_{\rm T} = 1.5$ K. Assuming the gas is optically thin, this implies a mean column density of $N_{\rm H} = 1.3 \pm 0.6 \times 10^{20}$ cm^{-2} and a mean internal H I number density of $n_{\rm H} \sim 0.07$ cm^{-3} if the shell is spherical.

3.1.   GSH 242-03+37 Physical Properties

The physical properties of GSH 242-03+37, such as radius, mass, expansion velocity, and expansion energy were estimated by Heiles (1979). Our values are only slightly different from those. Both our values and Heiles' values, where different, are given in Table 1.

Expansion velocities for shells are usually estimated as half of the total measured velocity width, Δv, of the shell. The full velocity width of GSH 242-03+37, through the center of the shell, is approximately $\Delta v = 25$ km s^{-1}. Because of the relationship between distance and radial velocity, there is a complicated coupling of the expansion velocity, $v_{\rm exp}$, and the velocity width due to the line-of-sight physical dimension of the shell, v_p. A simplistic way of de-coupling the expansion velocity and velocity width due to physical size is to use the velocity gradient, dv/dr, to estimate the contribution of the physical size to the total velocity width. Again using the Brand & Blitz (1993) rotation curve, we find that at $v = 42$ km s^{-1} along this line of sight $dv/dr \sim 10$ km s^{-1} kpc^{-1}. If the diameter of the shell along the line-of-sight is comparable to its diameter in the plane of the sky, then $v_p \sim 10$ km s^{-1}. We then make the simplifying assumption that the total velocity width is $\Delta v \approx 2v_{exp} + v_p = 25$ km s^{-1}, implying $v_{\rm exp} \approx 7$ km s^{-1}.

The expansion energy, E_E, of a shell is defined by Heiles (1979) to be the equivalent energy that would have been deposited at the center of the shell to account for the observed radius and expansion. The expansion energy, based on the calculations of Chevalier (1974) for supernova expansion, is $E_E = 5.3 \times 10^{43} \, n_0^{1.12} \, R_{\rm sh}^{3.12} \, v_{\rm exp}^{1.4}$, where n_0 is the ambient density measured in cm^{-3}, $R_{\rm sh}$ is in parsecs, $v_{\rm exp}$ is in km s^{-1}. This equation makes the extreme simplifying assumption that the ambient medium, n_0, into which the shell is expanding, is homogeneous with constant density. We know that this cannot be true on small scales, but for very large shells the density variations largely average out and the equation provides a

reasonable standard energy estimate with which to compare shells. For GSH 242-03+37, assuming $n_0 \approx 1$ cm^{-3}, the expansion energy is $E_E \sim 3.1 \times 10^{53}$ ergs. Another limitation of the expansion energy equation is that it does not account for energy lost to high latitudes by shell break-out. Therefore, for GSH 242-03+37 the expansion energy is only a lower limit. We note that our expansion energy estimate is about a factor of 10 lower than the value quoted in Heiles (1979). The difference between our value and Heiles' can be accounted for by our assumption of an ambient density of $n_0 \approx 1$ cm^{-3}, whereas Heiles (1979) uses $n_0 \approx 2$ cm^{-3}, and from the lower expansion velocity estimated here. If the average energy output of a single O or B star via its stellar winds and supernovae is $\sim 10^{51}$ ergs, then more than 300 massive stars are required to expand the shell to its current size. There are no known coveal stellar clusters of that size in the Milky Way, which suggests that GSH 242-03+37 was formed through the effects multiple generations of massive stars.

Age estimates for H I shells are also fraught with large uncertainties. Unless a powering source, such as an OB association, that can be aged independently is associated with the shell it is often impossible to accurately estimate the age of a shell. We can, however, estimate a shell's dynamic age based on models of the evolution of supernova remnants in the late radiative phase. In this case the dynamic age, t_6 in units of Myr for a shell of radius, $R_{\rm sh}$, given in pc and $v_{\rm exp}$ given in units of km s^{-1}, is given by $t_6 = 0.29\,R_{sh}/v_{\rm exp}$ (Cioffi et al. 1988). For GSH 242-03+37, the dynamic age is $t \sim 21$ Myr. Comparing with other known Galactic shells, GSH 242-03+37 is relatively old (Heiles 1979, 1984; McClure-Griffiths et al. 2002). Ultimately the lifetime of H I shells is limited by the development of instabilities along their walls and the onset of deformation and shear due to differential rotation in the Galactic plane. Both effects become significant at around 20 Myr (Dove et al. 2000; Tenorio-Tagle & Bodenheimer 1988). Differential rotation will distort the shell so that it no longer appears spherical. At a Galactocentric radius of 10.3 kpc this is a moderate effect; over 20 Myr a static shell of radius 1 kpc will distort to have an axial ratio in the plane of $\sim$1.5:1.

3.2.   GSH 242-03+37 Morphology

The three-dimensional morphology of GSH 242-03+37 is extremely interesting. One of the noteworthy aspects of the morphology is that the shell is not spherical, but has some "scalloped" structure along the edges as can be seen in Figures 1 and 6. The bases of these scallops are separated by several degrees or arcmin, or $\sim 400 - 500$ pc. In three locations, two at the bottom and one at the top, these arches are weaker or absent presenting extensions from the Galactic plane towards the halo. The three break-outs are at: $(l, b) = (245°2, +3°8), (243°0, -8°3)$ and $(236°5, -8°2)$. These break-outs or "chimneys" have

some vertical structures that clearly separate them from the ambient medium. At very low brightness temperatures (~ 1.5 K) the chimney structures are capped, each about 1.6 kpc from the center of the shell. These caps are marked on Figure 6, which is a channel image at $v = +45$ km s^{-1}. They are also visible in the channel images shown in Figure 1. Like the shell, the caps are visible over ~ 20 km s^{-1} of velocity space, which suggests that they are not only associated with the shell, but also physically extended. The structure and nature of these caps will be discussed in §4.3.

Figure 3 shows a slice across the shell in the longitudinal direction. The slice is taken at $v = 39.4$ km s^{-1}, $b = 0°.20$. The shell is clearly empty and the walls of the shell are very sharp. The walls show a brightness temperature contrast of 10 to 20 from the shell interior to the shell wall over one to two resolution elements, or $\sim 16 - 32$ pc. Referring to similarly strong shell walls in GSH 277+00+36, McClure-Griffiths et al. (2003) suggested that the sharpness of the walls is indicative of compression as associated with a shock.

Stacy & Jackson (1982) noted one cloud in the shell interior at $(l, b, v) = (242°.2, -4°.6, 36$ km s$^{-1})$, pointing out that it was unusual as one of the only clouds within a largely evacuated area. With the sensitivity of GASS it is clear that there is quite a lot of structure inside the shell, though in general it is only at the $T_b \sim 5$ K level. There are a number of interlocking rings throughout the shell interior. Most of these are relatively circular and noticeable over several velocity channels. The cloud cataloged by Stacy & Jackson (1982) appears to belong to a thin ring structure near the center of GSH 242-03+37, as shown in Figure 5. This ring is distinguished from the rest of the internal structure because it encloses an interesting region that is even more evacuated than the rest of the shell, appearing as a shell within the shell. This "mini-shell" is centered at $(l, b, v) = (242°.9, -2°.3, 45$ km s$^{-1})$ km s^{-1} and has an angular diameter of $\sim 3°.8$. The interior has lower brightness temperatures than the main void; the brightness temperatures associated with mini-shell are ~ 2 K inside the void, about a factor of two lower than in the main void, and $\sim 7 - 10$ K along the "walls". There are few regions in the Galactic plane that show such low brightness temperatures and most are associated with known H I shells.

Another particularly noticeable feature is the compact cloud a $(l, b, v) = (240°.9, +4°.9, 45$ km s$^{-1})$, which can be seen in several of the channel images presented in Figure 5. The unresolved cloud is surrounded by a ring of emission with a diameter of 2°. Also centered on this position, about 3 degrees away, is an arc of emission. These features, though noticeable, have no obvious physical explanation.

3.3. Comparison with other wavelengths

We have obtained publicly available data from the ROSAT all-sky survey maps of the diffuse X-ray background (Snowden et al. 1997). We compared the 1/4 keV, 3/4 keV and 1.5 keV emission with the H I distribution. There is clear evidence for $\frac{1}{4}$ keV excess emission in the shell interior. It would be surprising, however, if this excess were physically associated with shell. At 1/4 keV, unity optical depth corresponds to H I column densities of about 1×10^{20} cm^{-2} (Snowden et al. 1997), giving a mean free path for 1/4 keV X-rays of only ~ 65 pc. Even though the H I column density through the Puppis window is low, at the distance of GSH 242-03+37 the foreground H I column density is significant at $\sim 2 \times 10^{21}$ cm^{-2}. Examining the H I data cube, we find that the morphology of the X-ray excess agrees very well with the foreground H I shell, GSH 242-04-05 (Heiles 1979). It is therefore likely that the 1/4 keV X-ray excess emission traces hot gas in the foreground object, not in GSH 242-03+37.

The mean-free path for X-rays in the higher energy bands is much longer; 1.5 keV electrons have a mean free path of ~ 3 kpc (Snowden et al. 1997). Despite the potential detectability of higher energy X-rays, we find no correlation between the H I distribution and the 3/4 or 1.5 keV emission. The lack of harder X-ray features is not unexpected, however, because 3/4 and 1.5 keV emission suggests very hot gas with temperatures on the order of 10^7 K. Old large shells, like GSH 242-03+37 are not expected to have gas temperatures much higher than about 3.5×10^6 K (Mac Low & McCray 1988).

We have also compared the H I distribution to the velocity integrated Hα emission from the SHASSA survey of the Southern sky (Gaustad et al. 2001). Because of the low extinction towards this shell it should be possible to detect Hα emission to the 3.6 kpc distance of the shell. Unfortunately, because there is no velocity discrimination in the SHASSA data it is very difficult to distinguish foreground Hα features from features at the distance of the shell. We find very few obvious correlations between the H I at $v = 35 - 50$ km s^{-1} and Hα over the entire field of the shell. The only potential candidate for agreement is a faint Hα filament that lies just inside the H I mini-shell at $l = 243°$, $b = -2°.3$. This feature, however, is in a confused region and no definitive association can be made.

Finally, we have searched the FUSE catalog of O VI detections (Wakker at al. 2003) to determine if there is hot, high-latitude gas at the same velocity as GSH 242-03+37. Two O VI detections below the plane of the Galaxy are near GSH 242-03+37: the first towards PKS 0558-504 at 11 km s^{-1} and the second towards NGC 1705 at 29 km s^{-1}. However, neither of these pointings lie within the capped areas of the chimney outflows and the O VI is observed to be at lower velocities than that of the shell. Although it is likely that the shell is filled with hot gas, no connections between the FUSE O VI detections and the morphology of GSH

242-03+37 can be made at this time.

4. Discussion

GSH 242-03+37 is a remarkable structure. Its size, age, and morphology are all at the extreme range of observed Galactic shell parameters. The only known Galactic supershell to display similar properties is GSH 277+00+36 (McClure-Griffiths et al. 2003). The similarities between these two shells are intriguing. Both shells have radii of 350 - 500 pc and expansion energies on the order of 10^{53} ergs. Both are located far from the Galactic center at Galactocentric distances of ~ 10 kpc. The morphology of the two shells, particularly their walls and extended z structure, are strikingly similar (c.f. McClure-Griffiths et al. 2003, Figure 1). Although GSH 277+00+36 is a much less confusing structure than GSH 242-03+37, it exhibits similar chimney break-outs above and below the plane, as well as the same scalloped structure along the walls. The similar morphology of these two objects is intriguing and leads us to speculate that their large scale features may be dominated by common global Galactic phenomena, for example the H I scale height of the Galactic disk (R. Sutherland 2005, private communication), rather than local phenomena, such as the distribution of powering stars. It should be possible to determine which effects dominate with high resolution MHD simulations of supershell evolution. GSH 242-03+37, because it is closer, offers some advantages over GSH 277+00+36. In GSH 242-03+37 we can observe very weak chimney caps and explore the stellar content. Here we discuss some of the characteristics that are specific to GSH 242-03+37.

4.1. Stellar content

The stellar content of Galactic H I supershells is largely unknown. Most shells lie in the Galactic plane behind several magnitudes of visual extinction, precluding most optical stellar surveys. Infrared surveys, such as 2MASS, can probe to much greater distances than in the optical but the line-of-sight confusion of stars makes it difficult to associate specific stars with supershells. As it is, most of the known OB associations in the Galactic plane are at distances of less than 3 kpc. By contrast, most H I shells are at distances larger than 2 kpc because the confusion of gas at local velocities makes detecting shells difficult. Fortunately GSH 242-03+37 is located in the "Puppis Window" and benefits from numerous stellar studies. Kaltcheva & Hilditch (2000) recently compiled and updated the $uvby\beta$ photometry of luminous OB stars in the Puppis-Vela region, providing a nearly complete table of the stellar types and distances. We have extracted from their table all stars with projected

distances within 1 kpc of the center of the shell. For the region $234 \leq l \leq 252°$, $-7 \leq b \leq +7°$ there are 22 OB stars, of which the earliest is an O9 type star. These stars are plotted as crosses on Figure 4.

As one might expect for an old shell, there are very few massive stars in the center of the object, with the notable exception of a small cluster near $(l, b) = (242°, -5°)$. These stars belong to a cluster of O and B-type stars, which appear to lie along the rim of the internal mini-shell. The remaining stars are located near the shell walls. Along the right wall the stars appear to lie near the foci of the loops that characterize the scalloped structure of GSH 242-03+37. This coincidence seems to suggest that the stars near the edge of the shell are contributing to the continued expansion of the shell and determining the morphology of the walls. In addition, the stars trace the left-hand edge of the upper chimney wall, extending to $b = 6°.5$ or $z \approx 400$ pc at a distance of 3.6 kpc. The mean height for Galactic OB stars is only 90 pc (Miller & Scalo 1979), so OB stars at a height of 400 pc are unusual. One obvious explanation for their position is that they were formed out of dense material raised to high z by the shell.

A potential tracer of the past population of massive stars is the current population of pulsars. Perna & Gaensler (2004) examined the number of pulsars within several of the largest supershells in the Milky Way, including GSH 242-03+37. They compared the numbers of known pulsars with Monte Carlo simulations of the pulsar population to predict how many pulsars should be associated with a shell, assuming a multiple supernovae formation scenario for the shell. Although there are only 2 known pulsars within GSH 242-03+37, based on the current sensitivity of pulsar searches they predicted that there should be 7 pulsars within the shell. The known pulsars therefore provide very few constraints on the progenitor stars that may have formed the supershell.

4.2. The Mini-shell

Figure 5 shows the central region of GSH 242-03+37. The mini-shell (described in §3.2) is apparent at at $(l, b, v) = (242°.9, 2°.3, 45 \text{ km s}^{-1})$. If it, too, is at a distance of 3.6 kpc then the mini-shell has a radius of $R_{\text{sh}} \approx 120$ pc. There is no clear indication that the structure changes size with velocity although it is persistent over at least 7 km s^{-1} of velocity width. The shell is likely a stationary structure or one with a very small expansion velocity. From our data we can only estimate an upper limit to the expansion velocity of $v_{\text{exp}} \leq \Delta v/2 \sim 3$ km s^{-1}, which is less than the turbulent velocity of warm H I clouds, typically ~ 7 km s^{-1} (Belfort & Crovisier 1984). It is therefore impossible to distinguish the shell's expansion from random cloud motions in the ISM. For a stationary shell a rough estimate of the age of

the shell can be made from the sound crossing time for a 120 pc radius. Assuming $c_s \sim 10$ km s^{-1} for $T \sim 8000$ K H I, the age is $t \sim R_{\mathrm{sh}}/c_s = 12$ Myr.

How does the mini-shell relate to GSH 242-03+37? From the H I velocity channel images it appears as if the mini-shell is located within GSH 242-03+37. It is difficult to understand how a cool neutral shell could form within a mostly evacuated supershell. We have compared our estimates of the internal density of the supershell with the swept-up mass of the mini-shell showing that there is not enough gas in the supershell to form the mini-shell. From the measured column density along the mini-shell walls we estimate that the typical H I density in the walls is only $n_H \sim 0.4$ cm^{-3}, a factor of a few lower than typical ISM values (Dickey & Lockman 1990). This gives a swept-up mass for the shell of $\sim 7 \times 10^4$ M$_\odot$. If the shell were formed near the center of the main void, where we estimated that the typical H I density is only $n_H \sim 0.07$ cm^{-3}, then the total amount of mass enclosed in a sphere of radius 120 pc is only $\sim 1.2 \times 10^4$ M$_\odot$, a factor of six less than the swept-up mass of the shell. If the excess mass in the mini-shell came from swept-up ionized gas that had since recombined and cooled it would imply an ionized density of ~ 0.3 cm^{-3}. This is much higher than the typical ionized densities in shell interiors, which are usually on the order of $\sim 5 \times 10^{-3}$ cm^{-3} (Mac Low & McCray 1988). An alternative explanation is that the mini-shell is a very old structure that was formed through the stellar winds of the stars whose supernovae shocks eventually contributed to the large shell. In this case, the cool walls of the mini-shell might have been overtaken by the supernovae shocks, which subsequently expanded to much larger radii. The size of the mini-shell is approximately consistent with a late stage stellar wind bubble. A final suggestion is that the mini-shell formed not near the center of the shell, as it seems in the projected image, but at the edge or outside of the supershell where the gas densities should be higher. In order to be fully outside the main shell the mini-shell would require a systematic velocity that is $\sim 5 - 10$ km s^{-1} different from the LSR motion at its position. Given the dynamical nature of a large shell, that kind of motion is not unreasonable. Although it seems unlikely that the mini-shell formed in the interior of a swept-out supershell it is not possible with our data to distinguish between the latter two scenarios.

Along the lower wall of the mini-shell lies a small cluster of six O & B type stars (Kaltcheva & Hilditch 2000; Kaltcheva, Gredel, & Fabricius 2001). The cluster is at a distance of 3.2 ± 0.2 kpc and contains the stars: LS 538 (B0II), 514 (B1II) 507 (B0.5 III), 534 (B3), 528 (O9III), and 511 (B2) (Kaltcheva & Hilditch 2000). These stars are coincident with the brightest part of the mini-shell. Of these stars, only the later-type B2 and B3 stars are still on the main-sequence. If we assume coeval star formation, the age of the cluster must be between ~ 7 and 15 Myr (Schaller et al. 1992), which is comparable to the age estimate for the mini-shell. There are two possible scenarios to explain the presence of a stellar cluster

on the edge of this internal shell. The first is that the mini-shell formed from the stellar winds or supernovae of a single very massive star that was part of the stellar cluster. This seems unlikely if the stars are coeval, as the age of the stellar cluster is comparable to or less than the age of the shell. Alternately, the cluster may have formed out of gas compressed on the edge of the expanding mini-shell, causing a new generation of stars along the walls of the mini-shell. For as well as we can determine the ages of the shell and the cluster, this scenario seems most likely.

Many studies have searched for evidence of triggered star formation in supershells. In a recent study of the W3/W4 complex Oey et al. (2005) found evidence for three generations of star formation. They point out that, statistically, a hierarchical system of three or more generations of star formation is more suggestive of a causal relationship between the generations than a two generation system. In the GSH 242-03+37 system there is evidence of multiple epochs of star formation, contributing respectively to the ~ 21 Myr old supershell, the OB stars near the edges of the supershell, the mini-shell and the stellar cluster along the edge of the mini-shell. Whether these multiple epochs of star formation represent multiple generations or simply continuing star formation is not clear. Unfortunately, the ambiguous position of the mini-shell and the uncertainties in the shell ages makes it extremely difficult to identify three unique generations of star formation in the system. We therefore state that the system is *suggestive* of triggered star formation, but that the evidence is not conclusive.

4.3. Chimneys and Halo Clumps

GSH 242-03+37 has three chimney break-outs with the dominant one towards positive latitudes. All three chimneys are capped approximately 1.6 kpc above the center of the shell. The morphology of the positive latitude chimney in particular is reminiscent of the models of chimney formation, such as Mac Low, McCray, & Norman (1989); Tomisaka & Ikeuchi (1986). Mac Low et al. (1989) showed that for a superbubble expanding in a Galactic disk with an exponential atmosphere the shell will extend far beyond the Galactic mid-plane, developing a polar cap at $z \sim 1500$ pc. In the late stages of shell evolution gravitational acceleration dominates the dynamics of the slowly expanding shell and the polar cap should become Rayleigh-Taylor unstable and fragment. It is this fragmentation that allows hot gas filling the shell cavity to escape to the halo (Dove et al. 2000). As seen in Fig. 6 the upper cap of GSH 242-03+37 shows some evidence for fragmentation. There are a number of dense concentrations along the general arc of the cap, as well as some regions where the arc appears absent. We note however, that even with the sensitivity of GASS, the brightest features along this arc are only a few Kelvin in brightness temperature, so very faint portions

of the arc may not be detectable.

If, as these observations indicate, the polar caps of expanding supershells can reach heights of $z \sim 1500$ pc before fragmenting it raises questions about the ultimate fate of the fragmented caps and the expected size distribution for forming clouds. These questions have been addressed in a general sense in a variety of numerical simulations, (e.g. de Avillez 2000; de Avillez & Berry 2001). de Avillez (2000), for example, predicts that expanding shells should produce condensations of size 5 - 100 pc on timescales of tens of million years. The simulations explain the cloudlets in terms of expelled chimney gas that has cooled and recombined. GSH 242-03+37, on the other hand, seems to be producing cool clouds from the fragmented shell, a process that presumably takes place well before expelled chimney gas can cool.

The cool shell of GSH 242-03+37 appears to be fragmenting into cloudlets with sizes of a few tens of parsecs. The linewidths of these clumps are on the order of ~ 10 km s^{-1}, indicating thermal temperatures of $T \sim 10^3$ K or lower. We measure column densities (assuming they are optically thin) for these clumps of $N_H \sim$ few $\times 10^{19}$ cm^{-2}. If the clumps are roughly spherical, then their average H I number density is $n \sim 1$ cm^{-3} and their H I mass is ~ 100 M$_\odot$. The H I mass of the clumps is well below the dynamical mass limit to be gravitationally bound, which is $\sim 2 \times 10^5$ M$_\odot$ for a 10 pc cloud with a 10 km s^{-1} linewidth.

Are these clumps in pressure equilibrium with their surroundings? The thermal pressure of these clumps is $nT \sim 10^3$ cm^{-3} K. The thermal pressure of the lower halo at a z-height of 1.6 kpc is uncertain. By mass and volume the dominant component of the ISM at $z \sim 1.6$ kpc is warm ionized gas (Ferrière 2001), with a density of $\sim 4 \times 10^{-3}$ cm^{-3} and a temperature of ~ 8000 K (Reynolds 1991). We also know from observations of the soft X-ray background (Snowden et al. 1998) and O VI absorption (Savage et al. 2003), among others, that there is a significant diffuse, hot ($T \sim 10^{5-6}$ K) component to the lower halo gas. This component is difficult to observe directly but from FUSE O VI measurements Savage et al. (2003) suggest that it is distributed as a patchy, plane-parallel exponential with a scale height of ~ 2.3 kpc. The contribution of the hot, ionized medium to the thermal pressure of the lower halo is a matter for debate with estimates ranging from ~ 10 K cm^{-3} (Boulares & Cox 1990) to $\sim 10^3$ K cm^{-3} (Shull & Slavin 1994). It is generally agreed, however, that the presence of this medium, as well as its patchy nature are probably due to exhausting hot gas from supershells like GSH 242-03+37. Therefore, the best estimate for the thermal pressure of the ambient medium most likely comes from estimates of the thermal pressure in the interior of an evolved supershell.

It is not trivial to estimate the thermal pressure in the interior of GSH 242-03+37 because the shell has begun to break-out, releasing its pressure and also because the shell

is sufficiently evolved that radiative cooling is important in the interior. We can, however, roughly estimate the maximum internal thermal pressure before break-out, assuming an adiabatic interior where the internal density is dominated by mass evaporated from the cold dense shell (Mac Low & McCray 1988). The internal thermal pressure for an evolved spherical shell of age, $t_7 = t/10^7$ yr, formed with an energy deposition rate of $L_{38} \approx E_E/t/(10^{38} \text{ erg s}^{-1})$ is $nT = (1.4 \times 10^4 \text{ K cm}^{-3}) L_{38}^{14/35} n_0^{21/35} t_7^{-28/35}$ (Mac Low & McCray 1988). If, once again, we assume that the ambient density is $n_0 \sim 1 \text{ cm}^{-3}$, then the internal pressure is $\sim 1.4 \times 10^4 \text{ K cm}^{-3}$. Given that the shell has begun to break apart and that its z-height far exceeds its dimension along the Galactic plane, this pressure estimate is almost certainly too large but it provides a useful limit to the pressure around the clumps. We may therefore conclude that the clumps are likely in equilibrium or moderately pressure-supported by the hot gas from the shell.

We would like to know whether and for how long clouds created from the fragmentation of a shell could survive against evaporation due to heat flux from the ambient medium. If the ambient medium is indeed dominated by warm ionized gas, with $T \sim 8000$ K, then the classical thermal evaporation is extremely long when compared to the 20 - 30 Myr lifetime of the shell (Cowie & McKee 1977). Even if the ambient medium is dominated by the hot, diffuse gas of the shell interior, the evaporation time is ~ 35 Myr. We can expand on this estimation somewhat by following McKee & Cowie (1977) who consider the simple scenario of cool, spherical clouds embedded in a hot medium where the fate of the cloud is controlled by the effects of both radiative losses and incoming heat flux. Those authors provide analytic solutions to determine the critical radius, R_{cr} below which clouds evaporate and above which they condense material from the surrounding medium. The critical radius is determined solely by the pressure in the ambient medium. From Figure 2 in McKee & Cowie (1977) we estimate that the critical radius for $T \sim 8000$ K gas with a density of $\sim 4 \times 10^{-3} \text{ cm}^{-3}$ is ~ 3 pc. The clouds, however, are also affected by the very hot, tenuous medium interior to the shell. Even if this gas is at $\sim 10^6$ K with densities of 10^{-2} cm^{-3} the critical radius will be on the order of 15 pc and even lower for smaller ambient densities. Given these very crude assumptions it seems that the clouds should be near or above the critical radius for all expected temperatures in their environs. These clouds should therefore be relatively long-lived and may even condense matter onto themselves.

Another interesting question is what size scales should we expect to see represented from fragmenting caps. This of course depends on the instability process responsible for the fragmentation. If the shell cap fragments through classical Rayleigh-Taylor instabilities all size scales are expected to be represented, but the growth timescale of the instability is proportional to the square-root of the size scale so we should expect to see the smaller scales first. In addition, in the presence of a magnetic field a lower limit is applied to the size

of growing modes and also a fastest growing mode is established (McClure-Griffiths et al. 2003). In that case, the size scales observed in supershells may provide probes of the ambient medium.

In GSH 242-03+37 we observe large polar caps that appear to be breaking into clumps with radii on the order of tens of parsecs. The size, density, linewidths and z-height of these clumps is very similar to halo cloudlets detected by Lockman (2002) and those found in a recent study of the GASS pilot region (A. Ford et al. 2005a, in prep.). The origin of the Lockman (2002) clouds is still quite uncertain. If the polar caps of supershells like GSH 242-03+37 can break into small clumps with parsec or tens-of-parsec size scales these clumps should be much longer lived than the shell itself. Although these ideas are still rather speculative, the similarities of properties suggests that it would be worth pursuing the fragmenting shell model further. Some important questions to answer will be: how long can the clouds survive? what is their z distribution? and, given that they are massive compared to their surroundings, how long before they will drop back to the Galactic plane? We will address these questions in a future paper comparing the properties of halo cloudlets with simulations of the long term evolution of supershells (A. Ford et al. 2005b, in prep.).

5. Conclusions

We have presented new H I images of the Galactic supershell GSH 242-03+37 from the Galactic All-Sky Survey (GASS). GSH 242-03+37 is one of the largest shells in the Galaxy with a radius of $R_{sh} = 565 \pm 65$ pc. We show that the supershell is broken at the edge of the disk, both above and below the plane. The resultant structure has three "chimney" openings that are capped with very narrow filaments all situated ~ 1.6 kpc above the disk midplane. These "caps" are extremely reminiscent of the caps seen on expanding supershells in simulations, such as those by Mac Low et al. (1989) and Tomisaka (1998). In supershell evolutionary theories these shells should become Rayleigh-Taylor unstable and the polar caps break into clumps. The caps of GSH 242-03+37 appear to show clump structures with sizes on the order of 20 pc, which may indicate the onset of break-out. We estimate that clouds formed through this break-out may survive longer than the parent shell. The size, temperature and z-heights of these clouds are similar to the halo cloudlets detected near the disk in the inner Galaxy (Lockman 2002). We suggest that the Lockman cloudlets may be formed through the fragmentation of high-z supershell caps. All-sky surveys like GASS will provide an extremely valuable database for testing this idea. GASS will have the sky coverage, resolution and sensitivity necessary to detect and study the relationship of small-scale structures in the halo to structures in the Galactic disk.

We have searched catalogs of OB stars for massive stars in the vicinity of GSH 242-03+37. We find very few stars at the center of the shell, but there are 22 OB stars that lie near the internal edges of the shell, of which the earliest is an O9 type star. There are six OB stars with ages between 7 and 13 Myr (Kaltcheva et al. 2001) that lie along a small "mini-shell" that looks as if it is inside GSH 242-03+37. It is difficult to understand how a neutral shell could form in the evacuated cavity of GSH 242-03+37. We therefore suggest that it lies at the edge of the shell and that the OB stars were formed in material compressed along the walls of the mini-shell. The agreement between the main shell structure, the identification of 22 OB stars near the shell walls, the mini-shell and its corresponding cluster of young OB stars are suggestive, but not conclusive evidence for triggered star formation.

REFERENCES

Bajaja, E., Arnal, E. M., Larrarte, J. J., Morras, R., Poppel, W. G. L., & Kalberla, P. M. W. 2005, A&A, 440, 767

Barnes, D. G. et al. 2001, MNRAS, 322, 486

Belfort, P. & Crovisier, J. 1984, A&A, 136, 368

Boomsma, R., Oosterloo, T. A., Fraternali, F., van der Hulst, J. M., & Sancisi, R. 2005, in ASP Conf. Ser. 331: Extra-Planar Gas, 247

Boulares, A. & Cox, D. P. 1990, ApJ, 365, 544

Brand, J. & Blitz, L. 1993, A&A, 275, 67

Callaway, M. B., Savage, B. D., Benjamin, R. A., Haffner, L. M., & Tufte, S. L. 2000, ApJ, 532, 943

Chevalier, R. A. 1974, ApJ, 188, 501

Cioffi, D. F., McKee, C. F., & Bertschinger, E. 1988, ApJ, 334, 252

Cowie, L. L. & McKee, C. F. 1977, ApJ, 211, 135

de Avillez, M. A. 2000, MNRAS, 315, 479

de Avillez, M. A. & Berry, D. L. 2001, MNRAS, 328, 708

Dickey, J. M. & Lockman, F. J. 1990, ARA&A, 28, 215

Dove, J. B., Shull, J. M., & Ferrara, A. 2000, ApJ, 531, 846

Ehlerová, S. & Palouš, J. 2005, A&A, 437, 101

Ferrière, K. M. 2001, Reviews of Modern Physics, 73, 1031

Fitzgerald, M. P. 1968, AJ, 73, 983

Gaustad, J. E., McCullough, P. R., Rosing, W., & Van Buren, D. 2001, PASP, 113, 1326

Hatzidimitriou, D., Stanimirovic, S., Maragoudaki, F., Staveley-Smith, L., Dapergolas, A., & Bratsolis, E. 2005, MNRAS, 360, 1171

Heiles, C. 1979, ApJ, 229, 533

—. 1984, ApJS, 55, 585

Howk, J. C. & Savage, B. D. 1997, AJ, 114, 2463

Kalberla, P. M. W., Burton, W. B., Hartmann, D., Arnal, E. M., Bajaja, E., Morras, R., & Poppel, W. G. L. 2005, A&A, 440, 775

Kaltcheva, N., Gredel, R., & Fabricius, C. 2001, A&A, 372, 95

Kaltcheva, N. T. & Hilditch, R. W. 2000, MNRAS, 312, 753

Kim, S., Dopita, M. A., Staveley-Smith, L., & Bessell, M. S. 1999, AJ, 118, 2797

Lockman, F. J. 2002, ApJ, 580, L47

Mac Low, M. & McCray, R. 1988, ApJ, 324, 776

Mac Low, M., McCray, R., & Norman, M. L. 1989, ApJ, 337, 141

Mac Low, M.-M. & Ferrara, A. 1999, ApJ, 513, 142

Marlowe, A. T., Heckman, T. M., Wyse, R. F. G., & Schommer, R. 1995, ApJ, 438, 563

McClure-Griffiths, N. M., Dickey, J. M., Gaensler, B. M., & Green, A. J. 2002, ApJ, 578, 176

—. 2003, ApJ, 594, 833

McClure-Griffiths, N. M., Dickey, J. M., Gaensler, B. M., Green, A. J., Haynes, R. F., & Wieringa, M. H. 2000, AJ, 119, 2828

McKee, C. F. & Cowie, L. L. 1977, ApJ, 215, 213

Miller, G. E. & Scalo, J. M. 1979, ApJS, 41, 513

Müller, P., Reif, K., & Reich, W. 1987, A&A, 183, 277

Normandeau, M., Taylor, A. R., & Dewdney, P. E. 1996, Nature, 380, 687

Oey, M. S., Watson, A. M., Kern, K., & Walth, G. L. 2005, AJ, 129, 393

Perna, R. & Gaensler, B. M. 2004, ApJ, 606, 326

Rand, R. J., Kulkarni, S. R., & Hester, J. J. 1990, ApJ, 352, L1

Reynolds, R. J. 1991, in IAU Symp. 144: The Interstellar Disk-Halo Connection in Galaxies, 67–76

Reynolds, R. J., Sterling, N. C., & Haffner, L. M. 2001, ApJ, 558, L101

Savage, B. D., Sembach, K. R., Wakker, B. P., Richter, P., Meade, M., Jenkins, E. B., Shull, J. M., Moos, H. W., & Sonneborn, G. 2003, ApJS, 146, 125

Schaller, G., Schaerer, D., Meynet, G., & Maeder, A. 1992, A&AS, 96, 269

Shull, J. M. & Slavin, J. D. 1994, ApJ, 427, 784

Snowden, S. L., Egger, R., Finkbeiner, D. P., Freyberg, M. J., & Plucinsky, P. P. 1998, ApJ, 493, 715

Snowden, S. L., Egger, R. J., Freyberg, M. J., McCammon, D., Plucinsky, P. P. ., Sanders, W. T., Schmitt, J. H. M. M., Trümper, J., & Voges, W. 1997, ApJ, 485, 125

Stacy, J. G. & Jackson, P. D. 1982, A&AS, 50, 377

Staveley-Smith, L., Wilson, W. E., Bird, T. S., Disney, M. J., Ekers, R. D., Freeman, K. C., Haynes, R. F., Sinclair, M. W., Vaile, R. A., Webster, R. L., & Wright, A. E. 1996, Publications of the Astronomical Society of Australia, 13, 243

Tenorio-Tagle, G. & Bodenheimer, P. 1988, ARA&A, 26, 145

Tomisaka, K. 1998, MNRAS, 298, 797

Tomisaka, K. & Ikeuchi, S. 1986, PASJ, 38, 697

Williams, D. R. W. 1973, A&AS, 8, 505

Table 1.   Basic parameters for GSH 242-03+37

Parameter	Value
Center l	$243°$
Center b	$-1\overset{\circ}{.}6$
Central v_{LSR}	$+42$ km s^{-1}
Distance	3.6 ± 0.4 kpc
Radius	565 ± 65 pc
Velocity FWHM	25 km s^{-1}
v_{exp}	7 km s^{-1}(20 km s^{-1})[a]
E_{E}	3×10^{53} ergs (1.6×10^{54} ergs)

[a]Values given in brackets are from (Heiles 1979) and are only given where they differ significantly from the values determined here.
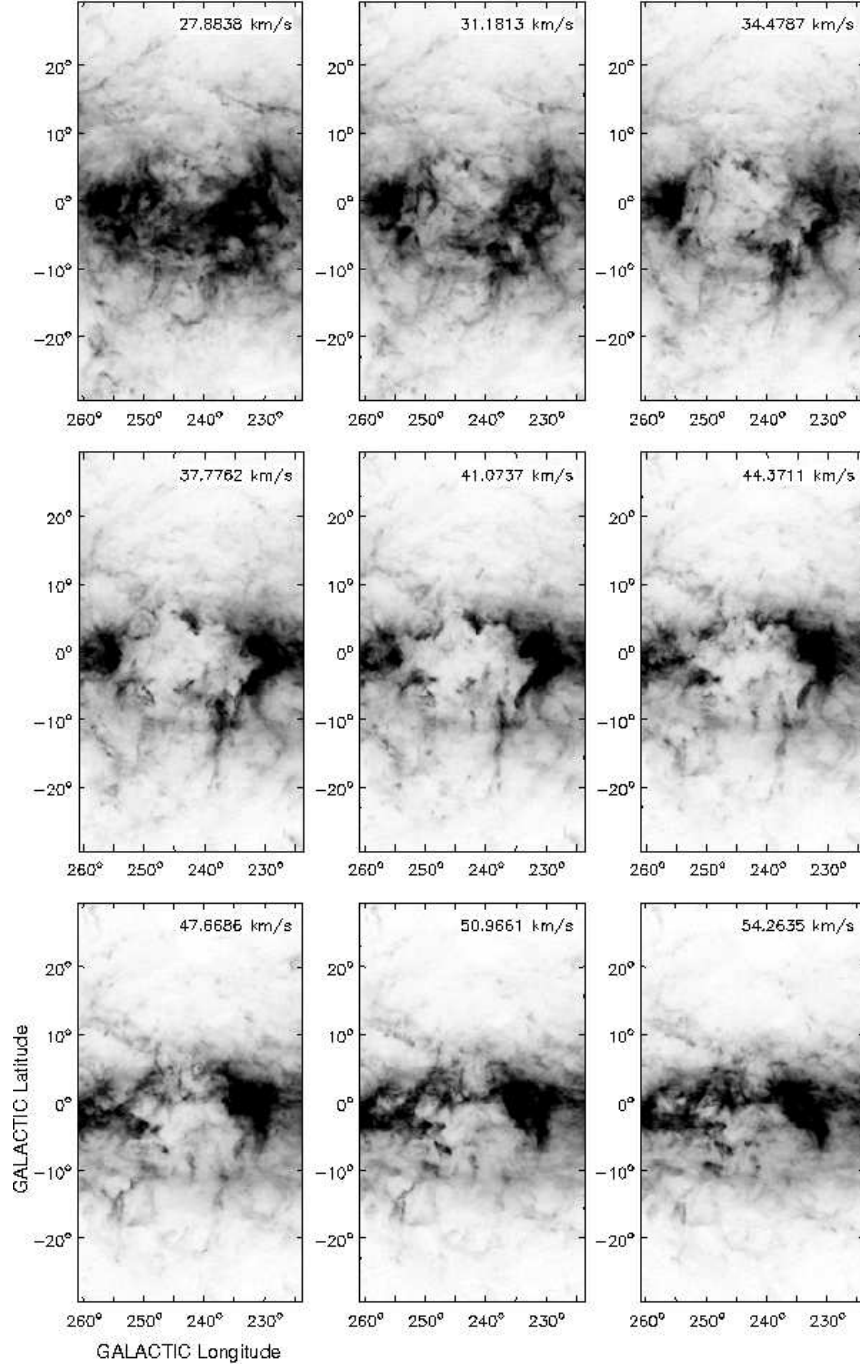
Fig. 1.— H I velocity channel images of GSH 242-03+37. Every fourth velocity channel between $v = 27.9$ km s^{-1} and $v = 54.3$ km s^{-1} is displayed. The LSR velocity of each channel is shown in the upper right corner of each panel. The grey scale has a scaling power cycle of -1 and goes between 0 (white) and 50 K (black). The expanding shell develops slowly from the first panel to its widest point near $v = 42$ km s^{-1}. The rear wall is apparent near $v = 54$ km s^{-1}.
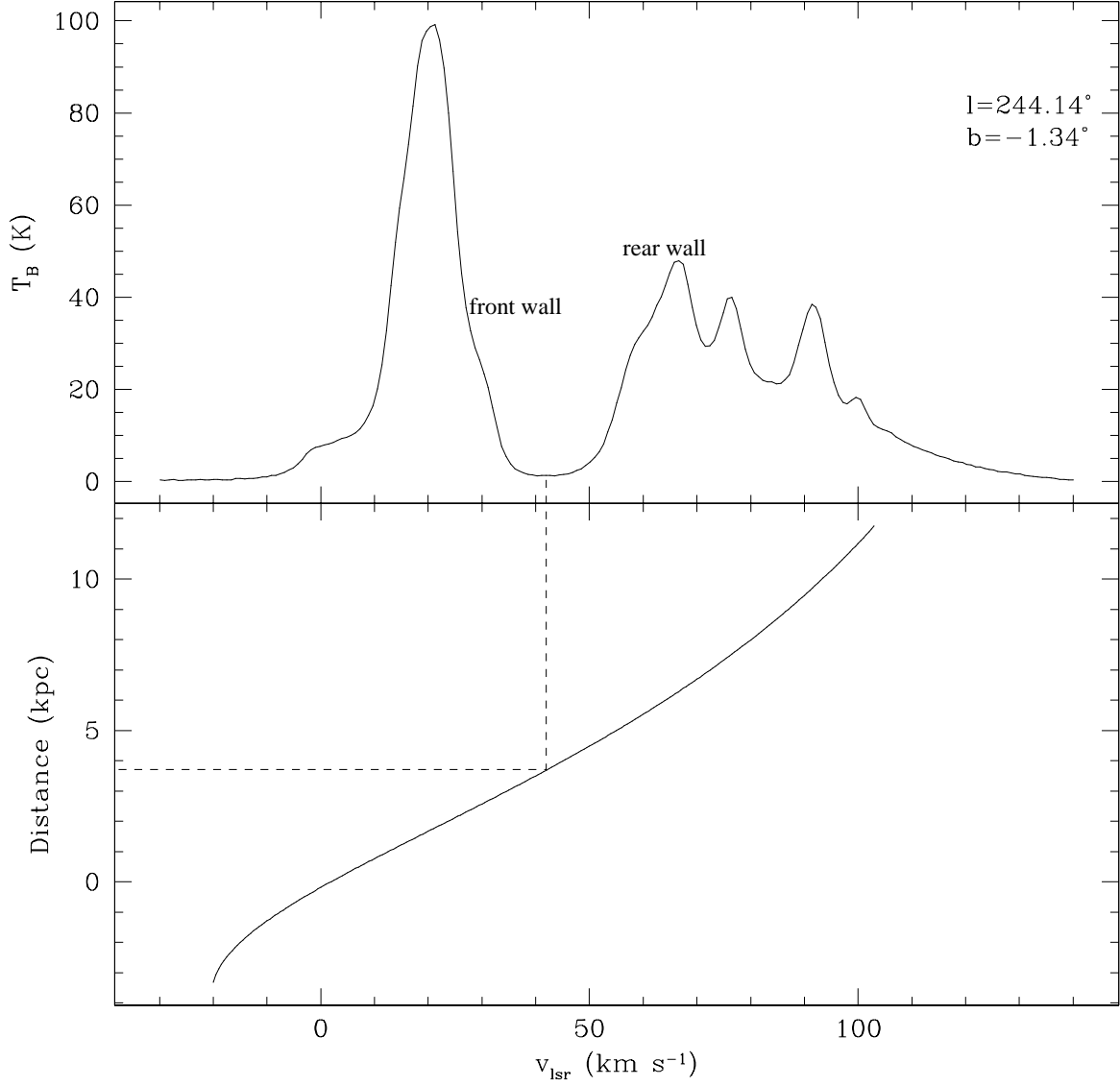
Fig. 2.— Velocity profile through the center of GSH 242-03+37, showing the deep well of the shell at $v = 42$ km s^{-1} and the peaks for its front and rear caps. The profile was extracted at $l = 244°14$, $b = -1°34$. The bottom panel shows the velocity-distance relation for this line of sight as defined by the (Brand & Blitz 1993) rotation curve. The kinematic distance of the shell center is at $d \approx 3.6$ kpc.
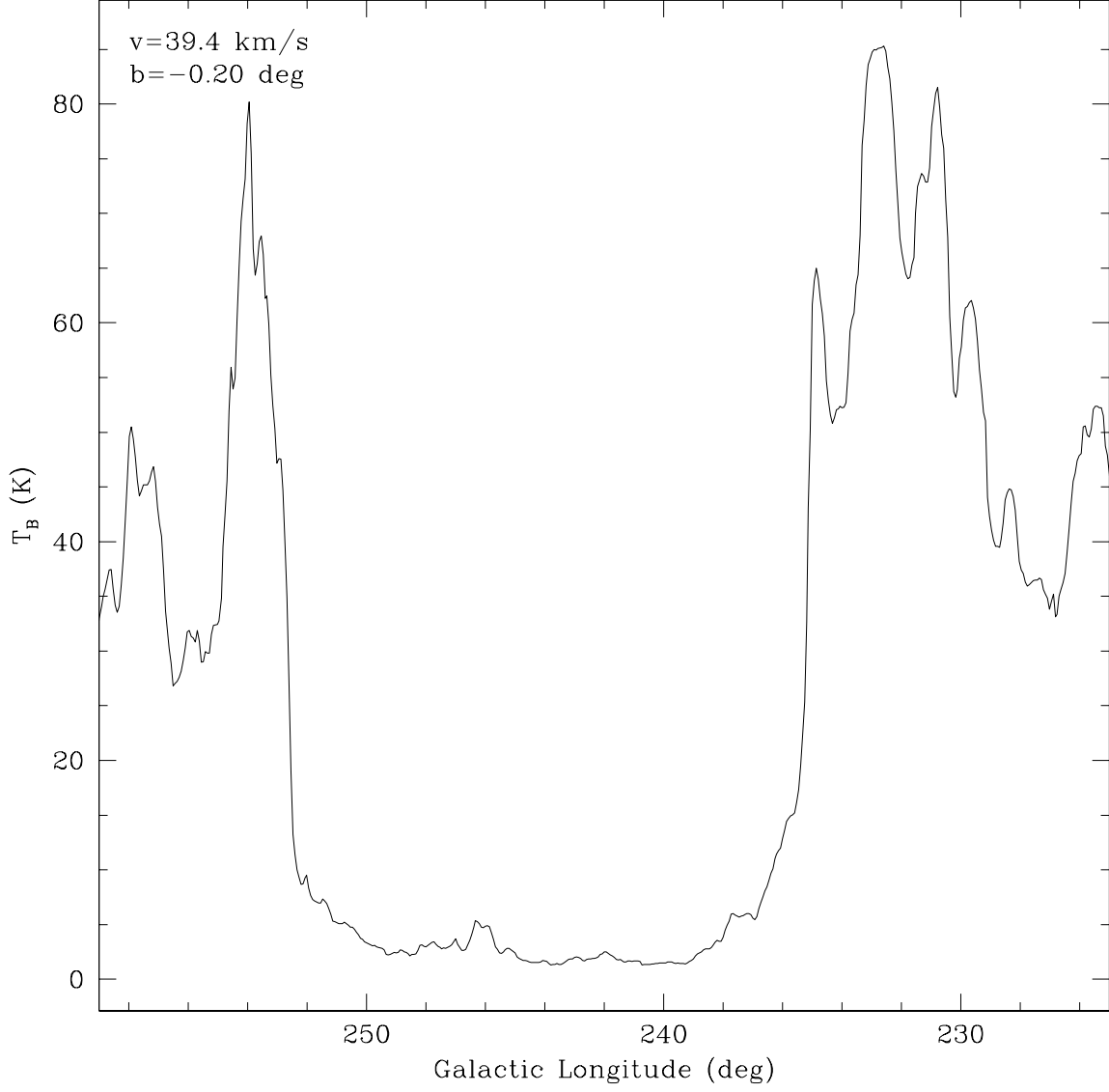
Fig. 3.— Galactic longitude slice across GSH 242-03+37 at $b = 0°.20$, $v = 39.4$ km s^{-1} showing the sharp walls and deep void of the shell center. The interior of the shell is quite empty with mean brightness temperatures of $T_b = 4 \pm 1.5$ K with low level structure. The sharp walls are indicative of a shell formed by compression.
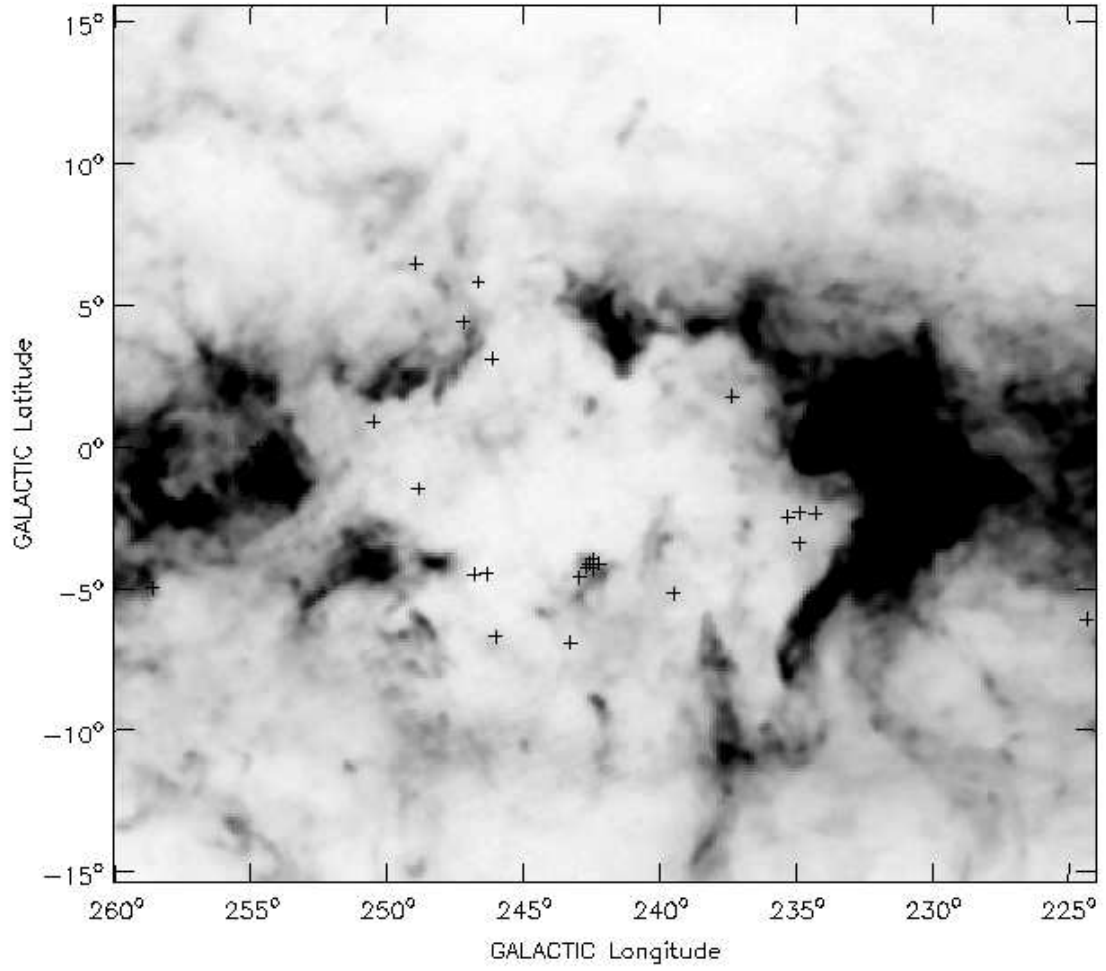
Fig. 4.— H I velocity channel image of GSH 242-03+37 at $v = 45.3$ km s^{-1}. The grey scale in this image has a scaling power of -0.4 and runs between 0 K (white) and 40 K (black). Stars from Kaltcheva & Hilditch (2000) located in the volume of the shell are plotted as crosses.
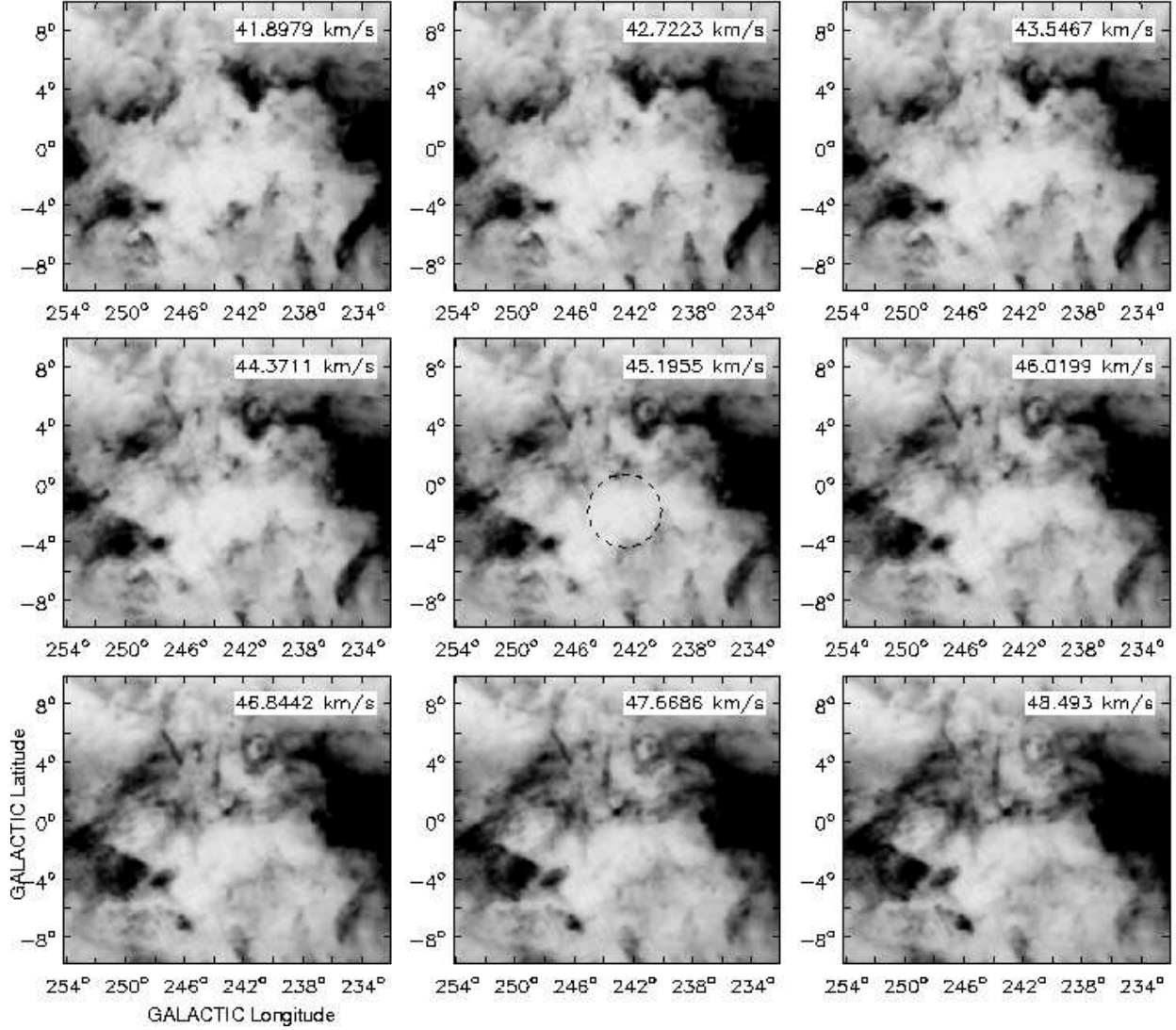
Fig. 5.— The central region of GSH 242-03+37. The grey scale runs from 0 K to 40 K with a scaling power cycle of -1. The image shows the "mini-shell", as a thin ring surrounding a void of $3°\!.8$ diameter centered on $l = 242°\!.9$, $b = -2°\!.3$. The mini-shell is outlined with a dotted line in the center panel. The shell does not change size with velocity, but is apparent across at least 6.5 km s^{-1} of velocity width.
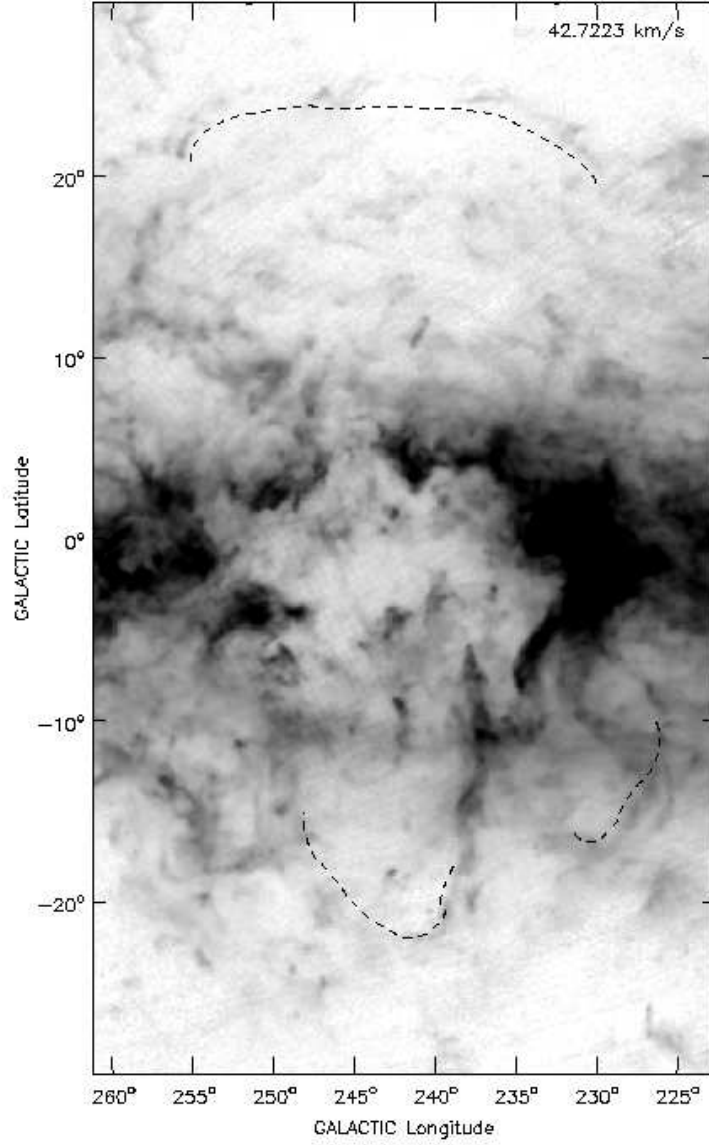
Fig. 6.— H I velocity channel image of GSH 242-03+37 at $v = 45.3$ km s^{-1}. The grey scale in this image is logarithmic and scaled between 0 K (white) and 45 K (black). The caps of the chimneys are marked with dotted lines. The most obvious cap is visible above the shell. All caps are located ~ 1.6 kpc from the center of the shell.